Applied Surface Science 349 (2015) 485–495

Contents lists available at ScienceDirect

Applied Surface Science

journal homepage: www.elsevier.com/locate/apsusc

New insight into electrochemical-induced synthesis of $NiAl_2O_4/Al_2O_3$: Synergistic effect of surface hydroxyl groups and magnetism for enhanced adsorptivity of Pd(II)

N.F.M. Salleh [a], A.A. Jalil [a,b,*], S. Triwahyono [c], J. Efendi [d], R.R. Mukti [e], B.H. Hameed [f]

[a] Department of Chemical Engineering, Faculty of Chemical Engineering, Universiti Teknologi Malaysia, 81310 UTM Johor Bahru, Johor, Malaysia
[b] Centre of Hydrogen Energy, Institute of Future Energy, Universiti Teknologi Malaysia, 81310 UTM Johor Bahru, Johor, Malaysia
[c] Department of Chemistry, Faculty of Science, Universiti Teknologi Malaysia, 81310 UTM Johor Bahru, Johor, Malaysia
[d] Department of Chemistry, Universitas Negeri Padang, Jl. Prof. Hamka, Air Tawar, Padang, West Sumatera, Indonesia
[e] Division of Inorganic and Physical Chemistry, Faculty of Mathematics and Natural Science, Institut Teknologi Bandung, Jl Ganesha No 10, Bandung 40132, Indonesia
[f] School of Chemical Engineering, Engineering Campus, Universiti Sains Malaysia, 14300 Nibong Tebal, Penang, Malaysia

ARTICLE INFO

Article history:
Received 1 April 2015
Received in revised form 5 May 2015
Accepted 8 May 2015
Available online 16 May 2015

Keywords:
$NiAl_2O_4$ spinel
Electrosynthesis
Isomorphous substitution
Adsorption
Pd^{2+} ions

ABSTRACT

A new promising adsorbent, Ni supported on γ-Al_2O_3 was prepared in a simple electrolysis system (Ni/Al_2O_3-E) in minutes and was compared with the sample prepared by a physical mixing method (Ni/Al_2O_3-PM). The adsorbents were characterized by XRD, TEM, FTIR, ^{27}Al MAS NMR, XPS, and VSM. The results showed that besides NiO nanoparticles, a $NiAl_2O_4$ spinel was also formed in Ni/Al_2O_3-E during the electrolysis via the dealumination and isomorphous substitution of Ni^{2+} ions. In contrast, only agglomerated NiO was found in the Ni/Al_2O_3-PM. Adsorption test on removal of Pd^{2+} ions from aqueous solution showed that the Pd^{2+} ions were exchanged with the hydrogen atoms of the surface–OH groups of both adsorbents. Significantly, the Ni/Al_2O_3-E demonstrated a higher adsorption towards Pd^{2+} ions than Ni/Al_2O_3-PM due to its remarkably higher degree of magnetism, which came from the $NiAl_2O_4$. The use of 0.1 g L^{-1} Ni/Al_2O_3-E gave the maximum monolayer adsorption capacity (q_m) of 40.3 mg g^{-1} at 303 K and pH 5. The Ni/Al_2O_3-E showed high potential for simultaneous removal of various noble and transition metal ions and could be also used repetitively without affecting the high adsorptivity for Pd^{2+} ions. This work may provide promising adsorbents for recovery of various metals as well as other materials for such related applications.

1. Introduction

Palladium (Pd) is one of the potentially toxic trace metals that is widely used in electrical industries, such as telephone relays, printed circuits, grids for electronic tubes, and electrodes for high-quality sparkplugs [1]. Incidentally, indiscriminate discharge of industrial waste without proper control creates an important environmental problem for aquatic systems. Due to its non-degradable properties, it tends to bio-accumulate in the food chain; the entrance of elevated doses of Pd(II) into the blood causes asthma, allergy, and rhino-conjunctivitis. In contrast, great interest has also been devoted to the extraction and recovery of this precious metal because of the increasing industrial demand and its limited resources [2]. Accordingly, several technologies have been developed for the effective removal of Pd ions from industrial wastewater, such as chemical precipitation, solvent extraction, electrolysis, membrane filtration, ion exchange, and adsorption [3]. However, most of these methods require high capital cost and energy consumption. Among them, adsorption is the most efficient method and is widely used for wastewater treatment due to its simplicity, low cost, and capacity for recycling and/or regeneration [4]. However, discovering an efficient alternative adsorbent to replace biomasses, carbon, and polymeric materials is indeed a real challenge because of the complex chemistry of metal ions [5].

Mixed metal oxide spinels with the general structure AB_2O_3 have long been a topic of interest because of their usefulness as magnetic materials, pigments, catalysts, and refractory materials [5–7]. For instance, nickel aluminate ($NiAl_2O_4$) is a transition

* Corresponding author at: Department of Chemical Engineering, Faculty of Chemical Engineering, Universiti Teknologi Malaysia, 81310 UTM Johor Bahru, Johor, Malaysia. Tel.: +60 7 5535581; fax: +60 7 5588166.
E-mail address: aishah@cheme.utm.my (A.A. Jalil).

http://dx.doi.org/10.1016/j.apsusc.2015.05.048
0169-4332/

metal spinel, in which its preparation is worth studying due to the large surface area and high stability [4]. Many methods have been explored, such as impregnation, co-precipitation, the sol–gel method, thermal reaction, and microwaves [8,9], but a simple, cheap, time-saving, and easily scaled method is still desired. $NiAl_2O_4$ is commonly used as a supporting catalyst for various metals and oxides, particularly for gas-phase catalytic reactions, as well as a potential material for internal reforming solid oxide fuel cell anodes. However, some works have reported the difficulty of reducing $NiAl_2O_4$ spinels for enhanced methanation [10]. This drawback has prompted researchers to find alternative uses for $NiAl_2O_4$. Similar properties having $NiFe_2O_4$ exhibited an efficient adsorption toward the reactive blue 5 [11], while modified Al_2O_3 has also shown the potential to remove various dyes. Thus, it is hypothesized that the $NiAl_2O_4$ that originates from Al_2O_3 will demonstrate good performance toward the adsorption of such toxic compounds. Moreover, reports on adsorption studies using $NiAl_2O_4$ spinels are still rare.

Previously, we reported a simple electrochemical method for preparing various metal oxide nanoparticles such as α-Fe_2O_3, ZnO, ZrO_2, and CuO supported on zeolites and mesoporous silica [12–15]. These catalysts were found to have a large potential in the decolorization of various dyes. Remarkably, herein a $NiAl_2O_4$ spinel structure was easily obtained in minutes when altering the electrolysis system for Ni supported on γ-Al_2O_3 (Ni/Al_2O_3-E). Its physicochemical properties were studied with XRD, TEM, FTIR, ^{27}Al MAS NMR, XPS, VSM, and surface area analyses. A comparison study was performed using the physical mixing method to mix the electrosynthesized NiO with γ-Al_2O_3 to produce Ni/Al_2O_3-PM. The promising performance shown by the Ni/Al_2O_3-E in the adsorption of Pd^{2+} ions from the aqueous solution demonstrates its potential application for the removal of various heavy metal ions. We also believe that this new finding of introducing the metal ions in a ceramic matrix could contribute to the design strategies for various catalysts for other reactions. The equilibrium isotherms, kinetics, and thermodynamics studies, proposed mechanisms, removal selectivity of various metal ions, and reusability are also thoroughly discussed.

2. Experimental

2.1. Materials

The γ-Al_2O_3 was purchased from Sigma–Aldrich. *N*,*N*-Dimethylformamide (DMF) was purchased from Merck Sdn. Bhd. Malaysia, and naphthalene was obtained from Fluka Sdn. Bhd., Malaysia. Sodium hydroxide (NaOH), hydrochloric acid (HCl), $Pd(Cl_4)$, $Pb(NO_3)_2$ ($HAuCl_4$), $Zn(NO_3)_2$, (H_2PtCl_6) and $Cu(NO_3)_2$ (C.I. 52015 for microscopy) were obtained from Merck. The platinum (Pt) and nickel (Ni) plate cells were obtained from Nilaco Metal, Japan. All reagents were of analytical grade and were used as received. Deionized water was used for the preparation of the pH solution and adjustments to the pH were performed using a 0.1 M HCl and NaOH solution.

2.2. Adsorbents preparation

The experimental procedures of synthesis of NiO were similar to those reported in the literature [16–18]. A DMF solution (10 mL) containing 0.1 M tetraethylammonium perchlorate was electrolyzed in the presence of a naphthalene mediator (6 mmol) in a normal one-compartment cell fitted with a Pt plate cathode (2 cm × 2 cm) and Ni plate anode (2 cm × 2 cm) at a constant current density of 120 mA/cm^2 under a nitrogen atmosphere at 273 K. After electrolysis, the mixture was impregnated, oven dried overnight at 378 K, and calcined at 823 K for 3 h to yield a black powder (NiO) for characterization and adsorption testing.

The Ni/Al_2O_3-E adsorbent was prepared by using the same procedure except for the addition of the Al_2O_3 (2 g) prior to electrolysis, and a green powder was obtained as the final product. For Ni/Al_2O_3-PM the NiO obtained from electrolysis above was mixed physically with Al_2O_3. The required weight percent of the NiO supported on Al_2O_3 and the time required for complete electrolysis was calculated based on Faraday's law of electrolysis:

$$t = \left(\frac{F}{I}\right)(Z \times n) \quad (1)$$

where t = total time for the constant current applied (s); F = 96,486 C mol^{-1}, which is the Faraday constant; I = the electric current applied; z = the valency number of ions of substances (electrons transferred per ion); and n = the amount of substance (no of moles, liberated $n = m/M$). For instance, the 3 wt% Ni/Al_2O_3-E was prepared in about 7 min.

2.3. Materials characterization

The crystalline structures of the adsorbents were studied by XRD recorded on a D8 ADVANCE Bruker X-ray diffractometer using Cu Kα radiation at a 2θ angle ranging from 3° to 90°. The phases were identified with the aid of the Joint Committee on Powder Diffraction Standards (JCPDS) files.

The textural properties (i.e., specific surface area, external surface area, micropore area, micropore volume, pore volume, and pore diameter) were determined from nitrogen adsorption–desorption isotherms at liquid nitrogen temperature using a Micromeritics ASAP 2010 instrument. The surface area was calculated with the BET method, and pore distributions were determined by the Barrett–Joyner–Halender (BJH) method whereas the micropore area, micropore volume, and external surface area were estimated by *t*-plots.

Transmission electron microscopy (TEM) was carried out using a JEOL JEM-2100F microscope. The samples were ultrasonically dispersed in acetone and deposited on an amorphous and porous carbon grid. Fourier transform infrared spectroscopy (FT-IR-PerkinElmer Spectrum GX FTIR Spectrometer) was performed using the KBr method with a scan range of 400–4000 cm^{-1}. The optical absorption properties of the adsorbents were obtained using UV–vis/DRS (PerkinElmer Spectrophotometer) in the range of 200–800 nm at room temperature.

Prior to measurement, all the samples were degassed at 110 °C to 0.1 Pa. ^{27}Al MAS NMR spectra were recorded on a Bruker Solid NMR (JEOL 400 MHz) spectrometer using tetramethylsilane (TMS) as an external reference at room temperature. The chemical oxidation state of the Ni/Al_2O_3 adsorbent was determined using X-ray photoelectron spectroscopy (XPS) conducted on a Kratos Ultra spectrometer equipped with a Mg Kα radiation source (10 mA, 15 kV) in the range of 0–800 eV. The powdered sample was pressed into a small Inox cylinder and analyzed inside an analysis chamber at 1×10^{-10} Pa during data acquisition. To correct the energy shift due to surface charging of the samples, the binding energy of the C1s peak at 284.5 ± 0.1 eV was taken as the internal standard.

The vibrating sample magnetometer (VSM) was used to study the magnetic properties. Magnetic hysteresis of the samples up to a field of 16 kOe were recorded using a Vibrating Sample Magnetometer (VSM-5S, TOEI Industry Co., Japan) at room temperature (297 K).

2.4. Adsorption study

In order to study the adsorptivity of the adsorbent Ni/Al_2O_3, the batch adsorption experimental procedure was applied for the

adsorption of Pd. The solution of Pd was prepared by dilution 1000 mg L^{-1} in distilled water. Then this experiment was conducted by adding 0.03 g of adsorbent in 250 mL beaker containing 150 mL of various concentrations of Pd solution (10–100 mg L^{-1}). The sample pH (2–12) was adjusted to the desired value with 0.1 M NaOH and 0.1 M HCl. The solutions were stirred at 400 rpm using magnetic stirrer to reach equilibrium. During the process, aliquots of 2 mL were withdrawn at pre-determined time intervals and centrifuge before the concentrations of Pd were analyzed by Atomic absorption spectroscopy (AAS). Various amounts of adsorbents (0.1–1.33 g L^{-1}) were used in the experiment to study the effect of adsorbent dosage. For effect of temperature, different temperature ranges from 303 to 323 K were studied. In order to reduce the measurement errors in the experiments, each set of experiments were done in triplicate. Then the equilibrium adsorption capacity, q_e (mg g^{-1}) was calculated by following equation,

$$q_e = \frac{C_0 - C_e}{m} \times V \quad (2)$$

where C_0 and C_e are the initial and equilibrium concentration (mg L^{-1}) respectively, m is the adsorbent weight (g) and V is the volume of Pd aqueous solution (L).

For the kinetics studies, the adsorbent (at a dosage of 0.1 g L^{-1}) was placed in contact with the five different initial concentrations of Pd solution. The agitation speed was kept constant (500 rpm), and analyses of the solutions were carried out using the same procedure as in the adsorption study. Meanwhile for thermodynamic study, the adsorbent (at a dosage of 0.1 g L^{-1}) was placed in three different temperature of Pd solution. The next procedures were prepared by similar procedure as mention above.

2.5. Multi-metal cations and reusability of the adsorbent

Multi-metal cation adsorption of Ni/Al_2O_3-E was examined in the presence of the following coexisting cations Pt^{4+}, Pb^{2+}, Au^{3+}, Zn^{2+} and Cu^{2+}. A sample containing a mixture of Pd^{2+} with the aforementioned cations was prepared at pH of 5 and 303 K. Concentration of each cation was maintained at approximately 10 mg L^{-1} and 200 mg L^{-1}.

3. Results and discussion

3.1. Structural and morphological properties

The Ni loaded onto Al_2O_3 by electrolysis (Ni/Al_2O_3-E), and by the physical mixing method (Ni/Al_2O_3-PM) were subjected to XRD in order to study their phase structure. The diffractogram are shown in Fig. 1A in the range of $2\theta = 10–80^\circ$, and compared with the bare NiO and γ-Al_2O_3. Fig. 1A(a) shows a wide-angle XRD pattern of the electrosynthesized NiO. A series of peaks were observed at 37.3°(1 1 1), 43.4° (2 0 0), 63.1° (2 2 0), and 75.4° (3 1 1), which could be indexed as a cubic NiO structure in comparison to the data from ICDD 04-002-0665. No other peak was found, indicating the purity of the NiO. The bare γ-Al_2O_3 demonstrates four distinct diffraction peaks at $2\theta = 19.5^\circ$, 36.6°, 45.8°, and 67.2°, which are indexed as (1 1 1), (3 1 1), (4 0 0) and (4 4 0) reflections, respectively (Fig. 1A(b)), representing a typical cubic structure of Al_2O_3 (JCPDS file number 29-0063) [19,20]. It could be observed that the peaks of Al_2O_3 were preserved in both Ni/Al_2O_3-E (Fig. 1A(c)) and Ni/Al_2O_3-PM (Fig. 1A(d)), indicating that the structure of the Al_2O_3 was retained despite the inclusion of Ni in both methods. Distinct peaks belonging to a face-centered cubic crystalline NiO were observed at 37.3°,

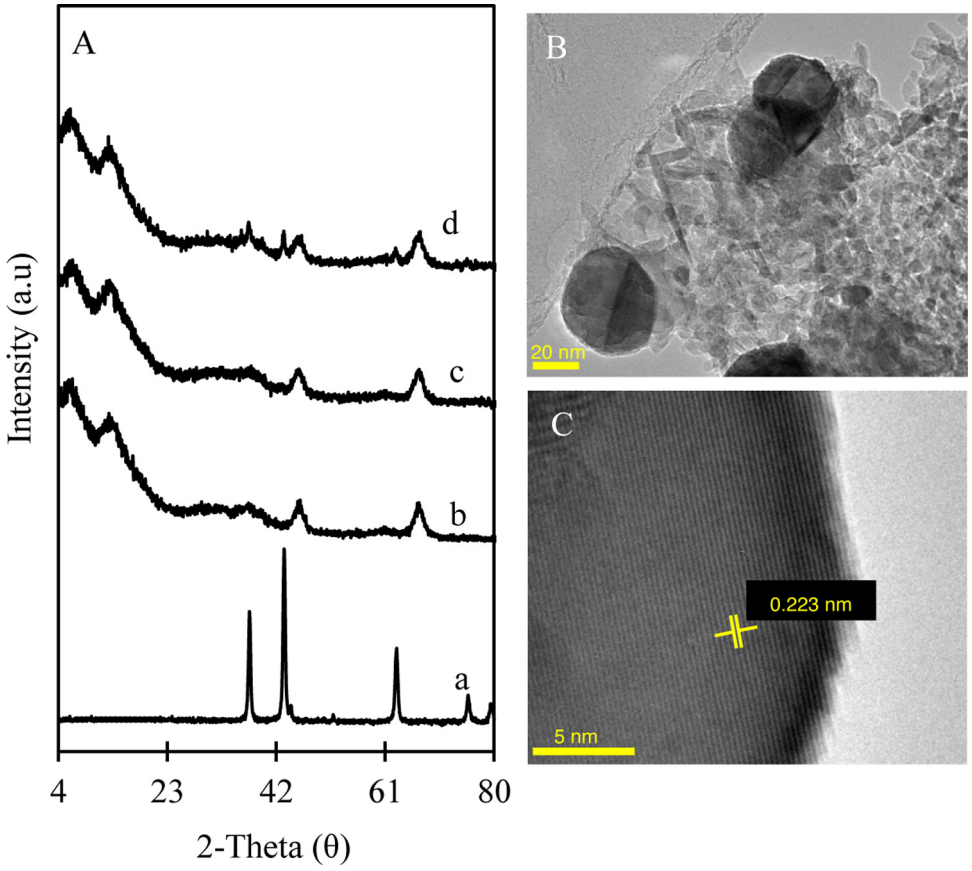

Fig. 1. (A) X-ray diffraction patterns of (a) NiO, (b) Al_2O_3, (c) Ni/Al_2O_3-E, (d) Ni/Al_2O_3-PM; TEM image of (B) Ni/Al_2O_3-E (C) *d* spacing for NiO on Ni/Al_2O_3-E.

Table 1
Textural properties.

Adsorbent	Surface area ($m^2\,g^{-1}$)	Pore volume ($mL\,g^{-1}$)	Pore diameter (nm)
Al_2O_3	200	0.567	7.24
Ni/Al_2O_3-E	190	0.499	7.24
Ni/Al_2O_3-PM	202	0.568	6.76

43.3°, and 63° for Ni/Al_2O_3-PM, signifying the presence of that species on the surface of the Al_2O_3. No NiO crystals were perceived on the Ni/Al_2O_3-E.

However, the presence of NiO nanoparticles on the Ni/Al_2O_3-E was detected with TEM, as shown in Fig. 1B and C, which appeared as black dots with an estimated outer diameter of 30–40 nm. An interplanar spacing shown in Fig. 1C was determined to be 0.223 nm, which implied the *d*-spacing of the (2 0 0) plane of cubic NiO. In addition, this value is consistent with the value calculated from the Bragg law in the XRD analysis, which was 0.219 nm.

3.2. Textural properties

Fig. S1 shows nitrogen adsorption–desorption isotherms and the corresponding pore size distribution plots (inset figure) of bare γ-Al_2O_3, Ni/Al_2O_3-E, and Ni/Al_2O_3-PM, while their detailed textural properties are shown in Table 1. A typical type IV isotherm was observed for each samples, which according to the Brunauer–Deming–Deming–Teller (BDDT) classification, it represented the condensation and evaporation steps for common mesoporous materials [21]. The framework porosity for all samples from 0.4 to 0.6 P/P_o indicates the porosity within the uniform channels of the template framework, while the textural porosity from 0.7 to 1 P/P_o shows the porosity that arises from the non-crystalline intra-aggregate voids and spaces formed by interparticle contact. The surface area of the Ni/Al_2O_3-E was slightly reduced, while the Ni/Al_2O_3-PM remained unchanged compared with the bare Al_2O_3 (Table 1), demonstrating that the introduction of Ni by electrolysis affected the structure of the Al_2O_3. The pore volume also shows the same trend, which suggests a good distribution of Ni species on the surface of the Ni/Al_2O_3-E and in the pore of the Al_2O_3, which caused the pore blockage, as confirmed by the pore size distribution shown in the inset figure in Fig. S1B. A similar phenomenon was reported for chromium supported on alumina [22]. The Ni/Al_2O_3-PM has a lower pore diameter compared with the Ni/Al_2O_3-E, which may be attributed to the dispersion of aggregated NiO around the pore mouth of Al_2O_3.

3.3. Vibrational spectroscopy

Fig. 2A shows the FTIR spectra of all samples in the region between 4000 and 400 cm^{-1}. It was observed that all samples exhibit bands attributed to –OH stretching (3417 cm^{-1}), water molecules retained in Al_2O_3 (1646 cm^{-1}), and overlapping metal peaks (1095–526 cm^{-1}) [23]. In comparison with the bare Al_2O_3, all the bands seemed perturbed when the Ni was loaded onto Al_2O_3 by both methods, especially for the Ni/Al_2O_3-E. The significant decrease in all bands of the Ni/Al_2O_3-E compared with the Ni/Al_2O_3-PM may be due to the ease with which dealumination occurs in the presence of ammonium salt in the electrolysis system. Subsequent isomorphous substitution of Ni^{2+} ions with hydrogen atoms from hydroxyl nests of the Al_2O_3 was proposed to form Al–O–Ni species. Similar observations were previously reported for metal ions that was isomorphously substituted into HY zeolite and mesoporous silica [12–14]. On the other hand, the slightly broad bands at 3417 and 558–549 cm^{-1} for Ni/Al_2O_3-PM as compared to bare Al_2O_3 most probably denotes the presence of excess numbers of Al–OH and Al–O–M, respectively. The dealumination accompanied by dehydroxylation of hydroxyl nests might be occurred during the calcination of Ni/Al_2O_3-PM at 823 K, which then increased the Al–O–Al bonds in the non-framework alumina [24].

For further study, the samples were evacuated at 673 K for 1 h prior to FTIR measurement to remove physisorbed water; the results of the hydroxyl groups located on the Al_2O_3 framework and those not on the framework are shown in Fig. 2B. The Ni/Al_2O_3-E and Ni/Al_2O_3-PM adsorbed Pd^{2+} ions were also compared and the details will be discussed later. Three main bands were observed, which indicated that the molecules were coordinately bonded to the different surfaces sites of the Al_2O_3, of which Al^{VI}–OH–Al^{VI} (3728 cm^{-1}), Al^{VI}–OH–Al^{IV} (3683 cm^{-1}), and –OH groups associated with non-framework Al_2O_3 (3610 cm^{-1}) [24]. A remarkable decrease of all –OH groups in the Ni/Al_2O_3-E were

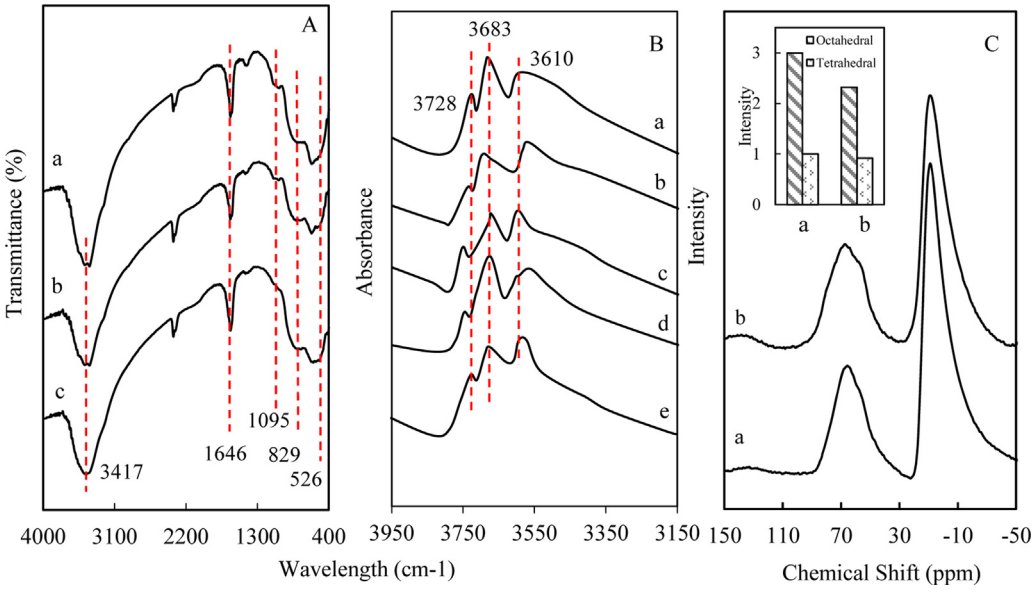

Fig. 2. FT-IR spectra for (A) KBr FTIR of (a) Al_2O_3, (b) Ni/Al_2O_3-E, (c) Ni/Al_2O_3-PM; (B) evacuated FTIR of (a) Al_2O_3, (b) Ni/Al_2O_3-E, (c) Ni/Al_2O_3-E adsorbed Pd^{2+} ions (d) Ni/Al_2O_3-PM, (e) Ni/Al_2O_3-PM adsorbed Pd^{2+} ions; (C) ^{27}Al NMR for (a) Al_2O_3, (b) Ni/Al_2O_3-E.

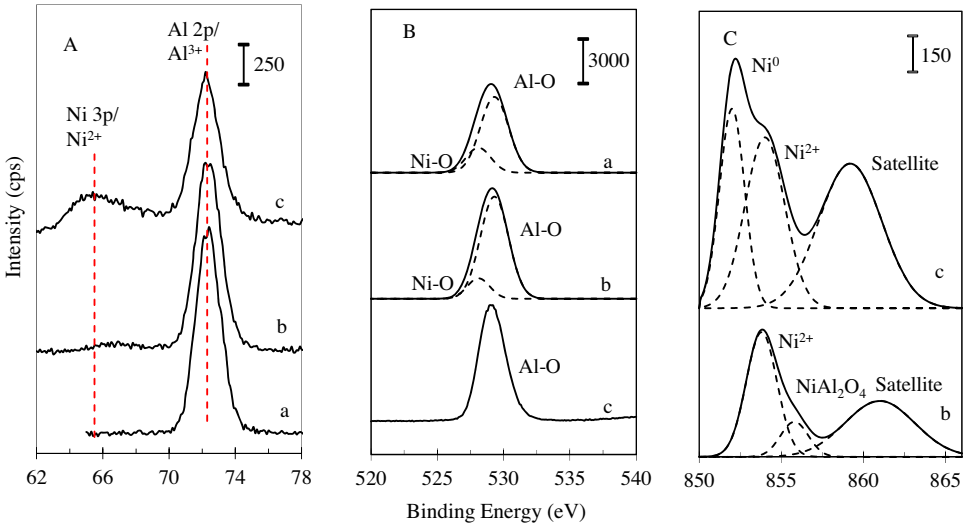

Fig. 3. XPS spectra of (A) Al 2p/Ni 3p (B) O1s (C) Ni 2p for (a) Al_2O_3 (b) Ni/Al_2O_3-E (c) Ni/Al_2O_3-PM.

observed (Fig. 2B(b)), confirming perturbation of the Al_2O_3 framework by dealumination and isomorphously substituted Ni cations during electrolysis [12]. However, in the case of the Ni/Al_2O_3-PM (Fig. 2B(d)), only the 3728 cm^{-1} band seemed decrease in intensity, supporting the dehydroxylation of hydroxyl groups for reformation of Al–O–Al bonds during the calcination.

Fig. 2C demonstrates the ^{27}Al MAS NMR spectra for tetrahedral (~70 ppm) and octahedral (~0 ppm) Al in the Ni/Al_2O_3-E compared with bare Al_2O_3. Based on the ratio of both resonance intensity difference to the bare Al_2O_3 (inset figure), the tetrahedral Al (AlO_4 structural unit, Al^{IV}) seems to retain its structure, but the octahedral (AlO_6 structural unit, Al^{VI}) form ratio is decreased. This result is in agreement with the evacuated FTIR data which indicated that the alterations for Al_2O_3 by electrolysis was readily occurred at the non-framework Al_2O_3. This restructuring is expected to give advantages in an adsorption of Pd^{2+} ions.

3.4. Chemical oxidation state determination

The samples were then subjected to XPS analysis in order to elucidate their exact structure. Fig. 3A(c) depicts the presence of outer-surface Ni^{2+} in the Ni/Al_2O_3-PM at the binding energies of 67 eV, which may belong to NiO [25]. The broad peak at 73.3 eV corresponds to Al 2p or Al^{3+} [26], which decreased in intensity in the following order: Al_2O_3 > Ni/Al_2O_3-E > Ni/Al_2O_3-PM. This result verified the dealumination during the electrolysis and calcination in both systems [27]. Similar to Fig. 3A, the amount of Al-O bond in the Ni/Al_2O_3-E is slightly higher than Ni/Al_2O_3-PM; the opposite was observed for Ni-O bonds, suggesting the isomorphous substitution of Ni^{2+} could suppressed the dealumination during calcination. Further investigation on Ni 2p spectra (Fig. 3C) confirmed that both Ni/Al_2O_3-E and Ni/Al_2O_3-PM possess peaks of Ni^{2+} and satellite, which are located at 854.4 and 860.5–862.5 eV, respectively [27]. Significantly, a peak belonging to $NiAl_2O_4$ was also seen in the Ni/Al_2O_3-E at 856.1 eV, while Ni/Al_2O_3-PM showed a peak at 852.1 eV, which corresponded to Ni^0 [28]. Thus, it could be stated that the introduction of Ni into Al_2O_3 via the physical mixing method obviously produced Ni^0 and NiO [29], while the electrolysis system clearly formed the NiO and $NiAl_2O_4$ spinel. The surface area analysis also verified the presence of NiO on the Ni/Al_2O_3-PM, shown by the decrease in its pore diameter. However, the presence of Ni^0 in the Ni/Al_2O_3-PM could not be supported by other analyses; this may be due to its small amount or the metal itself being covered by the NiO, as is the case for certain metals such as platinum [29]. In fact, the presence of NiO in the Ni/Al_2O_3-E was also confirmed by TEM images. Besides isormorphously substituted in the Al_2O_3 framework, abundance Ni^{2+} ions in the electrolysis system were also underwent reduction to produce Ni^0, which then being oxided to give the NiO by the calcination [17–19].

3.5. Adsorptive performance

The performance of all samples was examined for the adsorption of Pd^{2+} ions from an aqueous solution. As shown in Fig. 4A, the adsorption onto both pristine NiO and Al_2O_3 resulted in low adsorption capacity. It can clearly be observed that Ni/Al_2O_3-E exhibits the highest adsorptivity toward 10 mg L^{-1} Pd ions followed by Ni/Al_2O_3-PM, Al_2O_3, and NiO with an adsorption capacity of 7.0, 2.8, 2.5, and 1.8 mg g^{-1}, respectively. The VSM data shown in Fig. 4B confirmed that the $NiAl_2O_4$ in Ni/Al_2O_3-E possess a remarkably larger magnetic field to strongly attract the Pd^{2+} ions in comparison to agglomerated NiO-Ni^0 in the Ni/Al_2O_3-PM. In addition, the Pd^{2+} ions were also exchanged with the hydrogen atoms of bridging and non-framework –OH groups of Al_2O_3 in both samples, as verified by the decrease in intensity of the OH groups at band 3683 and 3610 cm^{-1}, respectively (Fig. 2B(c) and B(e)). A similar observation was reported in the literature for the adsorption of Pt(IV) and Pd(II) onto calcined dried aluminum hydroxide gel [30]. Thus, it could be dictated that the synergistic effect contributed by the strong magnetic attraction as well as ions exchange was a key factor in the efficient adsorption of Pd^{2+} ions using the Ni/Al_2O_3-E as compared to Ni/Al_2O_3-PM. While, the surface –OH groups and soft magnetic properties might be the main reason for the fair adsorption capacity achieved by Al_2O_3 and NiO, respectively. A proposed mechanism for the adsorption of Pd^{2+} ions by both adsorbents was illustrated in Fig. 5.

3.6. Equilibrium isotherm studies

Next, the equilibrium isotherm studies were performed using Ni/Al_2O_3-E in order to predict its adsorption uptake, which is one of the main parameters required for designing an optimized adsorption system. Four isotherm models, Langmuir, Freundlich, Temkin, and Dubinin–Radushkevich (D–R), were used to describe

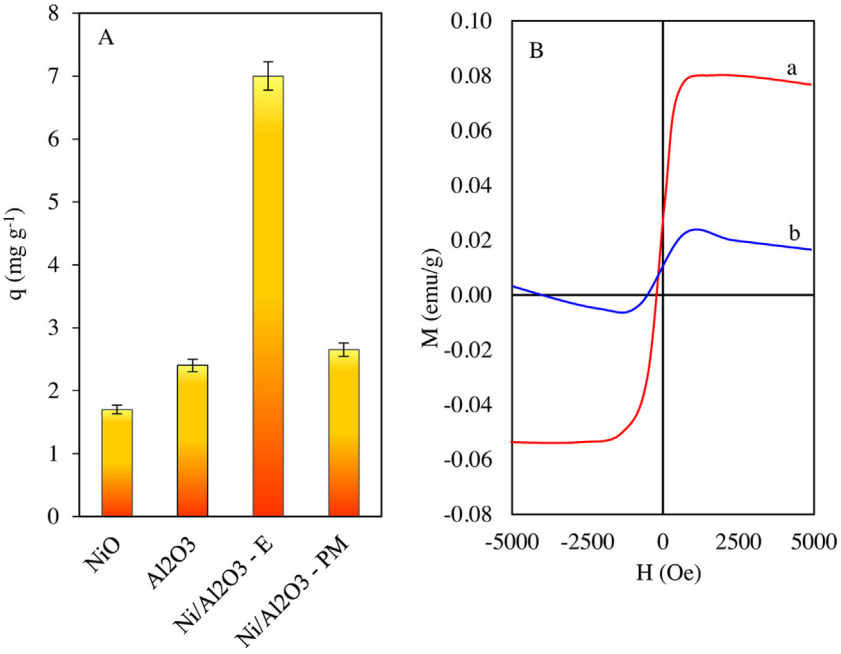

Fig. 4. (A) Performance of all samples on adsorption of Pd^{2+} ions (B) VSM spectra for (a) Ni/Al_2O_3-E (b) Ni/Al_2O_3-PM.

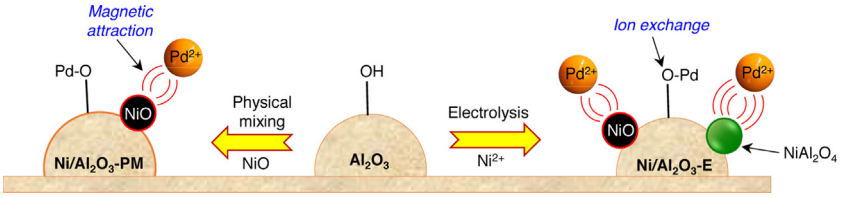

Fig. 5. A proposed mechanism for the adsorption of Pd^{2+} ions by Ni/Al_2O_3-E and Ni/Al_2O_3-PM.

the adsorption behavior of Pd^{2+} ions on the Ni/Al_2O_3-E; the equations used are as follows:

$$\text{Langmuir } q_e = \frac{q_m K_L C_e}{1 + K_L C_e} \quad (3)$$

$$\text{Freundlich } q_e = K_F C_e^{1/n_F} \quad (4)$$

$$\text{Temkin } q_e = B \ln A_T C_e \quad (5)$$

$$\text{Dubinin–Radushkevich } q_e = (q_s) \exp(-k_{ad}\varepsilon^2) \quad (6)$$

where q_e is the amount of Pd^{2+} ions adsorbed per gram of Ni/Al_2O_3-E ($mg\,g^{-1}$), q_m is the maximum adsorption capacity obtained from the isotherm ($mg\,g^{-1}$), C_e is the concentration of Pd^{2+} ions at equilibrium ($mg\,L^{-1}$), n_F is a heterogeneity factor, ε is the Polanyi potential, B (RT/b_T), b ($J\,mol^{-1}$) and A_T ($L\,g^{-1}$) are the heat of sorption and equilibrium binding constants, R is the gas constant ($8.314\,J\,mol^{-1}\,K^{-1}$), T is the absolute temperature (K), and K_L, K_F, A_T, and k_{ad} are related to the constants of the Langmuir, Freundlich, Temkin and D–R models, respectively. The non-linear plots of the isotherm models are shown in Fig. 6, while the extracted isotherm information is summarized in Table 2.

Among the four isotherms tested, the result showed strong evidence that the adsorption of Pd^{2+} ions onto Ni/Al_2O_3-E was satisfactory described by both Langmuir and Freundlich isotherm models. Similar trend was observed for the adsorption of tetramethylammonium hydroxide onto Y-type zeolite (NaY) [31]. The Freundlich model suggested that an adsorption is described as occurring heterogeneously on adsorption sites due to numerous adsorbent–adsorbate interactions. A heterogeneity factor (n_F) is used to identify the adsorption, i.e., whether it is linear ($n_F = 1$), a chemical process ($n_F < 1$) or a physical process ($n_F > 1$). The n_F obtained from this study was 1.63, indicating that adsorption is a physical process; the value was also classified as favorable adsorption because $1 < n_F < 10$. A relatively high correlation coefficient, R^2 value of Freundlich isotherm model depicted that a homogeneous surface with an equal energy and equally available sites was involved in the adsorption of Pd^{2+} ions onto Ni/Al_2O_3-E, with a

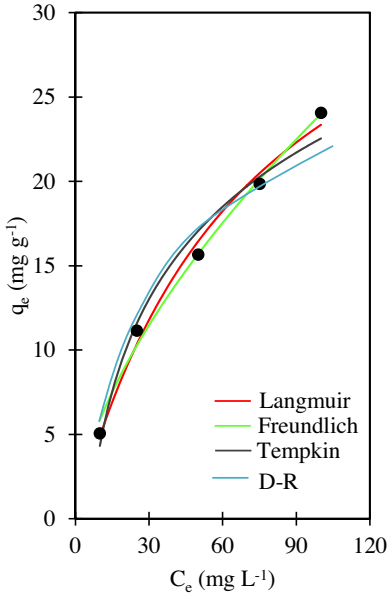

Fig. 6. Non-linear plots of isotherm models for Pd^{2+} ions removal onto Ni/Al_2O_3-E.

Table 2
Isotherm parameters for Pd^{2+} ions adsorption onto Ni/Al_2O_3-E.

Isotherms	Parameters	Values
Langmuir	q_m (mg g^{-1})	40.3
	K_L (L mg^{-1})	0.0139
	R^2	0.991
	R_L	0.418
Freundlich	K_F	1.43
	n_F	1.63
	R^2	0.993
Temkin	K_T (g^{-1})	0.173
	B (kJ mol^{-1})	7.91
	R^2	0.976
Dubinin	q_m	7.51
	K_{DR}	0.0121
	E (kJ mol^{-1})	6.43
	R^2	0.913

maximum adsorption capacity, q_m, of 40.3 mg g^{-1}. The R_L value is in the range of 0–1, indicating the favorability of the adsorption system. Compared with the data reported in the literature (Table 3), the Ni/Al_2O_3-E seems to be a potential adsorbent due to its relatively higher adsorption capacity for removing Pd^{2+} ions in a shorter contact time than various other materials.

The Temkin and D–R isotherms could also be considered to explain the nature and mechanism of the adsorption because of their fairly high value for R^2. The Temkin model was developed to describe the heat of adsorption and indirect adsorbent–adsorbate interactions on heterogeneous surfaces in adsorption systems. By ignoring the difference in concentration, the isotherm assumes that the adsorption heat of all molecules decreases linearly when the layer is covered. The positive value of parameter B, 7.91 kJ mol^{-1}, indicates the endothermic nature of the adsorption process.

The D–R model takes into account the porous structure of the adsorbent. Using this isotherm, the mean sorption energy, E, was calculated with the following equation:

$$E = \frac{1}{\sqrt{2K_{DR}}} \quad (7)$$

The E values obtained determine whether the process of adsorption proceeds by means of chemical (>16 kJ mol^{-1}), or physical adsorption (<8 kJ mol^{-1}) [32]. In addition, this energy is independent of temperature, but varies according to the nature of the adsorbent and the adsorbate. The calculated E value in this study was 6.43 kJ mol^{-1}, implying that adsorption occurred via physisorption. A similar phenomenon was observed in the adsorption of Cu(II) onto ion exchange resin [33].

3.7. Kinetics studies

Adsorption kinetics were studied to determine the rate and mechanism of adsorption [34]. In this study, the experimental data were fitted to three conventional kinetic models, namely the Lagergren pseudo-first order, the Ho pseudo-second order, and the Weber–Morris intraparticle diffusion model. The first two models are expressed as:

$$\text{Pseudo-first order } q_t = q_e(1 - e^{-k_1 t}) \quad (8)$$

$$\text{Pseudo-second order } q_t = \frac{q_e^2 k_2 t}{1 + q_e k_2 t} \quad (9)$$

where q_e is the amount of Pd^{2+} ions adsorbed per gram of Ni/Al_2O_3-E (mg g^{-1}), q_t is the adsorption capacity obtained at time t (mg g^{-1}), t is the time interval (min), and k_1 and k_2 are pseudo-first (min^{-1}) and pseudo-second order rate constants (mg g^{-1} min^{-1}), respectively. The kinetic parameters and correlation coefficients are listed in Table 4. It can be seen that the experimental data fit well with the pseudo-second order kinetics model (Fig. 7A), which was confirmed by the high value of R^2. In addition, the q_e values for the pseudo-second order were closer to the experimental data than the pseudo-first order. Similar adsorption characteristics have been reported for the adsorption of Cu, Ni, and Cr onto oak sawdust [35].

Next, the data were fitted with the intraparticle diffusion model to investigate the possible mechanism and rate controlling step of adsorption [21]. The equation used is as follows:

Intraparticle diffusion

$$q_t = k_{id} t^{1/2} + C_i \quad (10)$$

Table 3
Comparison of maximum adsorption capacities of various materials for Pd^{2+} ions.

Adsorbent	pH	Contact time (h)	Adsorption capacity (mg/g)	Refs.
Dried $Al(OH)_3$ gel	5	24	23.4	[43]
$Al(OH)_3$	6	0.5	8.5	[40]
Fe_3O_4	2.5	0.3	18.3	[44]
Nonylthiourea-coated Fe_3O_4	2.7	0.5	8.1	[30]
Al_2O_3 loaded aminophenol	6	24	11	[45]
Activated carbon	2	48	27	[46]
Bayberry immobilized collagen fiber	4	4	27.5	[47]
Amino functionalized silica gel	5	24	10.1	[48]
TiO_2	5.5	2	11.8	[49]
SBA-15	4	12	2.13	[50]
Ni/Al_2O_3-E	5	2	40.3	This study

Table 4
Kinetics parameters for Pd^{2+} ions adsorption onto Ni/Al_2O_3-E.

Adsorbent dosage	$q_{e,exp}$	Pseudo-first-order model			Pseudo-second-order model			Intraparticle diffusion		
(g)	(mg g^{-1})	$k_1 \times 10^{-2}$ (min^{-1})	$q_{1e,cal}$ (mg g^{-1})	R^2	$k_2 \times 10^{-3}$ (min^{-1})	$q_{2e,cal}$ (mg g^{-1})	R^2	$K_{id} \times 10^{-1}$ (mg g^{-1} min$^{-1/2}$)	C_i (mg g^{-1})	R^2
0.05	3.03	15.5	2.91	0.976	73.5	3.15	0.997	2.43	0.8821	0.764
0.04	3.56	22.6	3.32	0.971	100	3.54	0.994	2.67	1.16	0.711
0.03	5.20	25.9	4.86	0.958	79.3	5.16	0.986	3.87	1.77	0.693
0.01	14.1	17.5	12.8	0.967	18.9	13.7	0.994	10.8	3.99	0.777
0.005	23.7	9.71	22.5	0.979	5.61	24.7	0.997	19.9	5.31	0.831

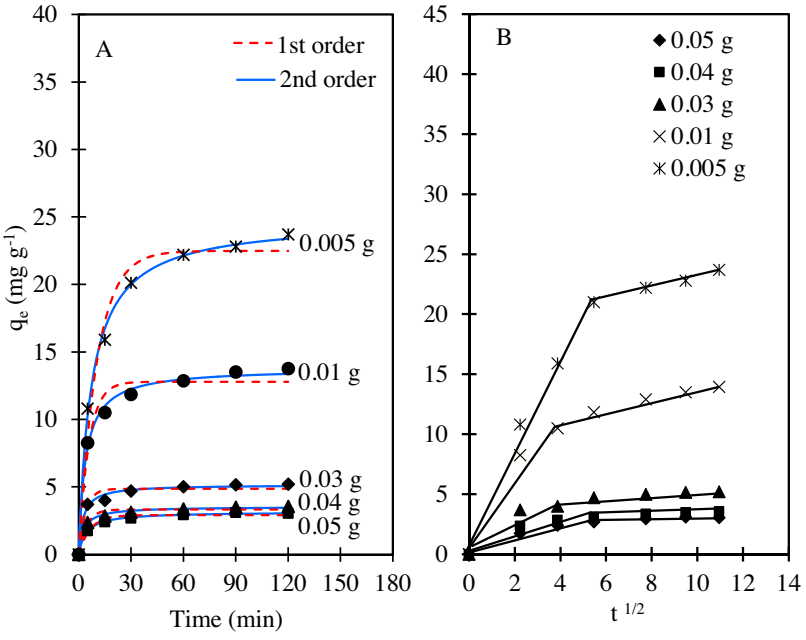

Fig. 7. (A) Non-linear plots of Pseudo-first and–second kinetics models (B) Weber–Morris intraparticle diffusion plot for Pd^{2+} ions removal onto Ni/Al_2O_3-E.

where k_{id} is a constant of intraparticle diffusion ($mg\,g^{-1}\,min^{-1/2}$), and C_i is the thickness of the boundary layer. The plots of q_t against $t^{1/2}$ for Ni/Al_2O_3-E at different adsorbent dosages are shown in Fig. 7B. It can be seen that the plots were not linear over the entire time period, but could be divided into 2 parts, suggesting that two steps were involved in the adsorption process: (1) an initial steeper line that might be attributed to an external mass transfer of Pd^{2+} ions from the boundary layer to the surface of the Ni/Al_2O_3-E, and (2) an upper linear portion attributed to intraparticle diffusion via micro- and mesopores of the Ni/Al_2O_3-E [36]. The initial external mass transport of Pd^{2+} ions was too rapid and then quickly slowed down, so that intraparticle diffusion became rate controlling. Table 4 shows the decreasing trend in q_e, k_{id}, and C_i as adsorbent dosage increased. The higher the dosage, the greater the adsorption surface sites, which then led to a thinner boundary layer, as well as increasing collisions between adsorbent molecules that lowered the intraparticle diffusion rate, k_{id}. In addition, this deterioration in the boundary layer thickness supports the physisorptional nature of the adsorption process. This relationship has been reported by Yadava et al. in relation to their study on the effect of temperature upon the boundary layer for the adsorption of Pb(II) ions on China Clay and Wollastonite [37].

3.8. Thermodynamic studies

Thermodynamic parameters were then calculated to further study the mechanism involved in the adsorption process. Experiments were conducted at 303, 313, and 323 K and the adsorption enthalpy (ΔH°), entropy (ΔS°), and Gibbs free energy (ΔG°) were calculated using the following equations:

$$\ln K_c = \frac{\Delta S^\circ}{R} - \frac{\Delta H^\circ}{RT} \quad (11)$$

$$K_c = \frac{C_e(\text{adsorbent})}{C_e(\text{solution})} \quad (12)$$

$$\Delta G^\circ = -RT\,\ln K_c \quad (13)$$

The linear form of the Van't Hoff equation (Eq. (11)) was plotted (Fig. 8A) to calculate the values of ΔH° ($kJ\,mol^{-1}$) and ΔS° ($J\,mol^{-1}\,K^{-1}$) for adsorption from the slope and intercept of $\ln K_c$ versus $1/T$, respectively. The thermodynamic parameters at three different temperatures are presented in Table 5. The positive ΔH° value confirmed the endothermic nature of the adsorption, which is in agreement with the B_T parameter in the Temkin isotherm model.

Similar trends were also observed for Cu(II), Pb(II), and Cd(II) using a low-cost bipolymeric sorbent [38]. The absolute magnitude of ΔH° is 26.1 $kJ\,mol^{-1}$, signifying an ion exchange process, as an enthalpy range of −24 to 38 $kJ\,mol^{-1}$ is generally considered as an ion exchange process [32]. Meanwhile, the positive value of ΔS° suggests an increase in randomness at the solid–solution interface, with some structural changes in the adsorbate and adsorbent during the adsorption process. The decreasing ΔG° values correlating with elevating temperature indicate a decrease in the practicality of adsorption at higher temperatures. The positive values of ΔG° at all temperatures indicates the non-spontaneous nature of the adsorption process of Pd^{2+} ions onto Ni/Al_2O_3-E, in which the system does gain energy from the surroundings. Similar phenomena have been observed in the adsorption of Hg(II), Pb(II), and Zn(II) onto montmorillonite clay [39].

Activation energy (E_a) is another important parameter in determining the type of adsorption. The rate constant of the pseudo-second-order kinetic model, k_2, was used to calculate E_a using the Arrhenius equation:

$$\ln k_2 = \ln A - \frac{E_a}{R}\left(\frac{1}{T}\right) \quad (14)$$

The slope of the linear plot of $\ln k_2$ versus $1/T$ gave a value for E_a (Fig. 8B). A more positive energy reflects the greater energy required to initiate adsorption. In fact, low activation energies (<40 kJ/mol) are characteristic of physisorption, while higher

Table 5
Thermodynamics parameters for Pd^{2+} ions adsorption onto Ni/Al_2O_3-E.

Temp (K)	$q_{e,exp}$ ($mg\,g^{-1}$)	ΔG ($kJ\,mol^{-1}$)	ΔH ($kJ\,mol^{-1}$)	ΔS ($kJ\,mol^{-1}\,K^{-1}$)	E_a ($kJ\,mol^{-1}\,K^{-1}$)
303	3.12	5.71	26.1	0.078	
313	7.98	3.25			74.3
323	14.9	2.14			

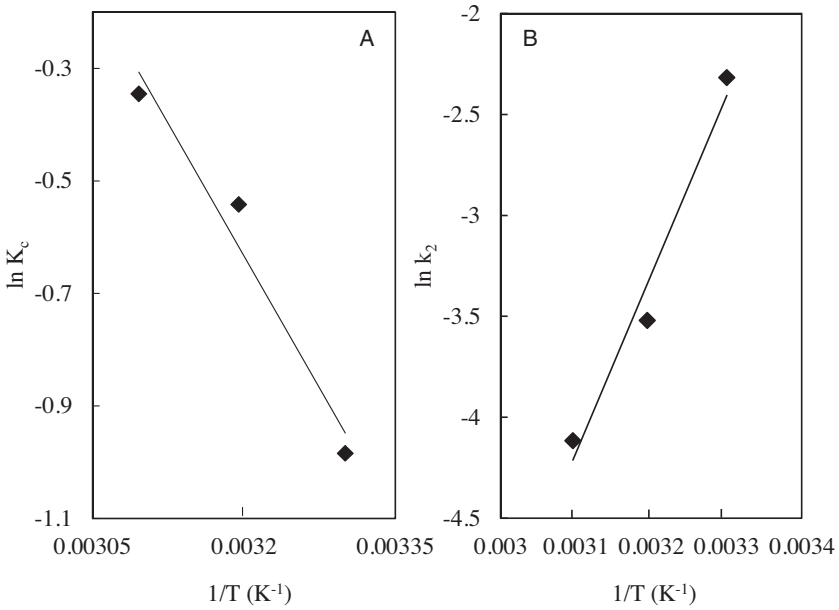

Fig. 8. (A) Plot of ln K_C versus $1/T$ for estimation of thermodynamic parameters and (B) plot of ln k_2 versus $1/T$ for estimation of E_a for the adsorption of Pd^{2+} onto $NiAl_2O_3$-E.

activation energies (>40 kJ mol^{-1}) are indicative of chemisorption, and a range between 0.2 and 80 kJ mol^{-1} represents the ion exchange for mesoporous materials [32]. The value of E_a (74.3 kJ mol^{-1} K^{-1}) falls into the second and third range, confirming that adsorption occurred in both chemisorption and ion exchange processes. Thus, the equilibrium isotherms, kinetics, and thermodynamic studies verified that physisorption, chemisorption, and ion exchange processes are involved in the adsorption of Pd ions onto the Ni/Al_2O_3-E.

3.9. Simultaneous removal of various metal ions

The removal of heavy metal ions in wastewater is becoming increasingly important and has attracted much attention among researchers. Along this line, herein the efficiency of Ni/Al_2O_3-E toward both nobel (Pd^{2+}, Pt^{4+}, Au^{3+}) and transition (Pd^{2+}, Pt^{4+}, Au^{3+}) noble metal ions was examined; the results are shown in Fig. 9A. A similar trend of removal was observed either for low or high concentrations, in which the removal efficiency was in the following order: Pd > Pt > Pb > Au > Zn > Cu. The higher selectivity for Pd^{2+} ions in comparison to other noble metal ions may be due to the geometry square planar of Pd^{2+}, which allows its fast adsorption, while more complex structures such as Pt^{4+} and Au^{3+} might require a longer time to be adsorbed. Similar phenomenon can be seen in the adsorption of platinum metal ions on other group metals (Pd, Pt, Rh) Fe_3O_4 [40]. In general, the competitive adsorption ability varies from one metal ion to another and is related to a number of factors such as molecular mass, ion charges, hydrated ionic radius, and the hydration energy of the metals [41]. In addition, the low competition of coexisting cations in respect to Pd^{2+} ions for the active sites on the Ni/Al_2O_3-E signify multi-surface adsorption [42].

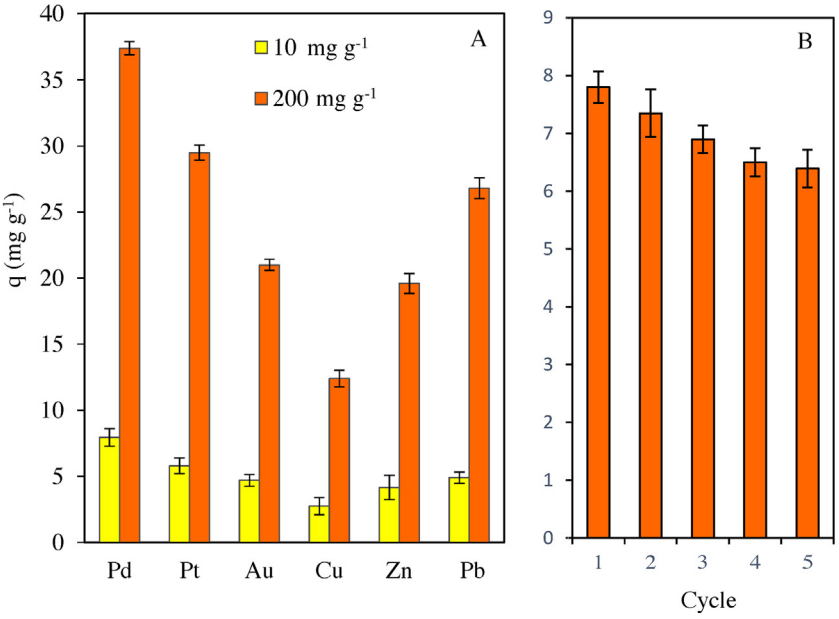

Fig. 9. (A) Effect of coexisting ions on Pd^{2+} ions removal. (B) Reusability of Ni/Al_2O_3-E for adsorption of Pd^{2+} ions during five cycles.

3.10. Reusability of the adsorbent

A repeated experiment was carried out using the Ni/Al_2O_3-E in order to study the stability of the adsorbent for Pd^{2+} ions (Fig. 9B). The initial concentration of Pd^{2+} ions was kept constant (10 mg L^{-1}) at pH 5 for 2 h of contact time, and the adsorbent was recycled after being washed with HNO_3 and calcined at 823 K for 3 h in every cycle. It can be observed that after five repeated experiments, the adsorbent was still active with only a reduction from 7.8 to 6.4 mg g^{-1} for the removal of Pd^{2+} ions. The heat treatment most probably induced the catalyst aggregation after several recycles, which caused a decrease in surface area and finally led to a decrease in adsorption efficiency [22].

4. Conclusion

In this study, a new promising adsorbent Ni supported on γ-Al_2O_3 (Ni/Al_2O_3-E) was synthesized using a simple electrolysis system and was compared with an adsorbent prepared with a physical mixing method (Ni/Al_2O_3-PM), which used the same electrolyzed NiO source. The physicochemical properties of the adsorbents were characterized by N_2 physisorption analysis, XRD, TEM, FTIR, ^{27}Al MAS NMR, XPS, and VSM. The FTIR data showed that the dealumination for the Ni/Al_2O_3-E occurred during the electrolysis and for Ni/Al_2O_3-PM occurred during the calcination. Then, subsequent isomorphous substitution of Ni^{2+} cations into the Al_2O_3 framework and dehydroxylation took place for the Ni/Al_2O_3-E and Ni/Al_2O_3-PM, respectively. The ^{27}Al MAS NMR spectra supported the perturbation of the extra-framework Al of the Ni/Al_2O_3-E as a consequence of the dealumination. The XRD results revealed the retention of the γ-A_2O_3 structure of both adsorbents after the introduction of Ni, as well as the presence of NiO on the Ni/Al_2O_3-PM. Further characterization using TEM showed the presence of NiO on the Ni/Al_2O_3-E. Furthermore, the XPS proved the presence of NiO in both catalysts, and also nickel aluminate ($NiAl_2O_4$) spinel and Ni^0 in the Ni/Al_2O_3-E and Ni/Al_2O_3-PM, respectively. The N_2 sorption analysis showed that the addition of Ni altered the surface area, pore volume, and pore diameter of both adsorbents. The performance test on the removal of 100 mg L^{-1} Pd^{2+} ions indicated that the Ni/Al_2O_3-E was the most potential adsorbent, giving the maximum monolayer adsorption capacity of 40.3 mg g^{-1} at 303 K and pH 5. The equilibrium data were evaluated using the Langmuir, Freundlich, Temkin, and D–R isotherm models, with the Freundlich model giving the best fit with the adsorption data. The adsorption kinetics were best described by the pseudo-second-order model. Thermodynamic studies showed that the adsorption was endothermic and not spontaneous at low temperatures. The adsorption was found to occur via magnetic attraction and also ion exchange of the Pd^{2+} ions with the hydrogen atom of the–OH groups of Al_2O_3. The VSM result verified that the presence of both NiO and $NiAl_2O_4$ on the $NiAl_2O_3$-E surface provided remarkably larger magnetic fields to attract Pd^{2+} ions compared with the agglomerated NiO-Ni^0 on the $NiAl_2O_4$-PM. The ability of the $NiAl_2O_4$-E to remove both noble and transition metals ions while retaining the higher selectivity for Pd^{2+} ions indicates its potential to be used in multi-surface adsorption of heavy metal ions in wastewater. The reusability studies indicated that the $NiAl_2O_4$-E can be used repeatedly without impacting its adsorption capacity. These results indicated the $NiAl_2O_4$-E had a good adsorption ability to remove heavy metal ions from the aqueous solution.

Acknowledgements

The authors are grateful for the financial support by the Research University Grant from Universiti Teknologi Malaysia (Grant No. 05H09), the awards of MyPhD Scholarship (Nur Fatien Muhamad Salleh) from Ministry of Higher Education, Malaysia, and to the Hitachi Scholarship Foundation for their support.

Appendix A. Supplementary data

Supplementary data associated with this article can be found, in the online version, at http://dx.doi.org/10.1016/j.apsusc.2015.05.048

References

[1] M.R. Awual, I.M. Rahman, T. Yaita, M.A. Khaleque, M. Ferdows, pH dependent Cu (II) and Pd (II) ions detection and removal from aqueous media by an efficient mesoporous adsorbent, Chem. Eng. J. 236 (2014) 100–109.
[2] V. Kumar, S. Srivastava, S. Umrao, R. Kumar, G. Nath, G. Sumana, P.S. Saxena, A. Srivastava, Nanostructured palladium-reduced graphene oxide platform for high sensitive, label free detection of a cancer biomarker, RSC Adv. 4 (2014) 2267–2273.
[3] Y. Meng, D. Chen, Y. Sun, D. Jiao, D. Zeng, Z. Liu, Adsorption of Cu^{2+} ions using chitosan-modified magnetic Mn ferrite nanoparticles synthesized by microwave-assisted hydrothermal method, Appl. Surf. Sci. 324 (2015) 745–750.
[4] X. Chen, K.F. Lam, K.L. Yeung, Selective removal of chromium from different aqueous systems using magnetic MCM-41 nanosorbents, Chem. Eng. J. 172 (2011) 728–734.
[5] B. Ismail, S.T. Hussain, S. Akram, Adsorption of methylene blue onto spinel magnesium aluminate nanoparticles: adsorption isotherms, kinetic and thermodynamic studies, Chem. Eng. J. 219 (2013) 395–402.
[6] W. Shangguan, Y. Teraoka, S. Kagawa, Simultaneous catalytic removal of NO(and diesel soot particulates over ternary AB_2O_4 spinel-type oxides, Appl. Catal. B 8 (1996) 217–227.
[7] L. Zhou, J. Xu, X. Li, F. Wang, Metal oxide nanoparticles from inorganic sources via a simple and general method, Mater. Chem. Phys. 97 (2006) 137–142.
[8] K.D. Becker, F. Rau, High temperature ligand field spectra in spinels: cation disorder and cation kinetics in $NiAl_2O_4$, Ber. Bunsen-Ges. Phys. Chem. 91 (1987) 1279–1282.
[9] Z. Boukha, C. Jiménez-González, B. de Rivas, J.R. González-Velasco, J.I. Gutiérrez-Ortiz, R. López-Fonseca, Synthesis, characterisation and performance evaluation of spinel-derived Ni/Al_2O_3 catalysts for various methane reforming reactions, Appl. Catal. B 158–159 (2014) 190–201.
[10] M. Khosravi, Eftekhar, Characterization and evaluation catalytic efficiency of $NiFe_2O_4$ nano spinel in removal of reactive dye from aqueous solution, Powder Technol. 250 (2013) 147–153.
[11] N.F. Jaafar, A.A. Jalil, S. Triwahyono, M.N.M. Muhid, N. Sapawe, M.A.H. Satar, H. Asaari, Photodecolorization of methyl orange over α-Fe_2O_3-supported HY catalysts: the effects of catalyst preparation and dealumination, Chem. Eng. J. 191 (2012) 112–122.
[12] N.W.C. Jusoh, A.A. Jalil, S. Triwahyono, H. Setiabudi, N. Sapawe, M.A.H. Satar, A.H. Karim, N.H.N. Kamarudin, R. Jusoh, N.F. Jaafar, Sequential desilication isomorphous substitution route to prepare mesostructured silica nanoparticles loaded with ZnO and their photocatalytic activity, Appl. Catal. A 468 (2013) 276–287.
[13] A.A. Jalil, M.A.H. Satar, S. Triwahyono, H. Setiabudi, N.H.N. Kamarudin, N.F. Jaafar, N. Sapawe, R. Ahamad, Tailoring the current density to enhance photocatalytic activity of CuO/HY for decolorization of malachite green, J. Electroanal. Chem. 701 (2013) 50–58.
[14] N. Sapawe, A.A. Jalil, S. Triwahyono, M.I.A. Shah, R. Jusoh, N.F.M. Salleh, B.H. Hameed, A.H. Karim, Cost-effective microwave rapid synthesis of zeolite NaA for removal of methylene blue, Chem. Eng. J. 229 (2013) 388–398.
[15] A.A. Jalil, N. Kurono, M. Tokuda, Facile synthesis of 2-arylpropenoic acid esters by cross-coupling using electrogenerated highly reactive zinc and a palladium catalyst, Synlett 12 (2001) 1944–1946.
[16] A.A. Jalil, N. Kurono, M. Tokuda, Synthesis of the precursor of anti-inflammatory agents by cross-coupling using electrogenerated highly reactive zinc, Synthesis 18 (2002) 2681–2686.
[17] R. Saravanan, V. Gupta, V. Narayanan, A. Stephen, Visible light degradation of textile effluent using novel catalyst ZnO/γ-Mn_2O_3, J. Taiwan. Inst. Chem. E 45 (2014) 1910–1917.
[18] A.A. Jalil, N. Kurono, M. Tokuda, Facile synthesis of ethyl 2-arylpropenoates by cross-coupling reaction using electrogenerated highly reactive zinc, Tetrahedron 58 (2002) 7477–7484.
[19] L. Krajczyk, P. Kraszkiewicz, L. Kepinski, Interaction of $Ce_{1-x}Er_xO_{2-y}$ nanoparticles with Al_2O_3, Mater. Chem. Phys. 151 (2015) 196–205.
[20] X. Tian, Q. Wu, K.M. Wong, C. Yang, W. Wang, X. Wu, Y. Wang, S. Zhang, Y. Lei, A simple technique for the facile synthesis of novel crystalline mesoporous ZrO_2-Al_2O_3 hierarchical nanostructures with high lead(II) ion absorption ability, Appl. Sufr. Sci. 284 (2013) 412–418.
[21] A.H. Karim, A.A. Jalil, S. Triwahyono, S.M. Sidik, N.H.N. Kamarudin, R. Jusoh, N.W.C. Jusoh, B.H. Hameed, Amino modified mesostructured silica nanoparticles for efficient adsorption of methylene blue, J. Colloid Interface Sci. 386 (2012) 307–314.

[22] M. Cherian, M.S. Rao, W.-T. Yang, J.-M. Jehng, A.M. Hirt, G. Deo, Oxidative dehydrogenation of propane over Cr_2O_3/Al_2O_3 and Cr_2O_3 catalysts: effects of loading, precursor and surface area, Appl. Catal. A 233 (2002) 21–33.
[23] R. Saravanan, H. Shankar, T. Prakash, V. Narayanan, A. Stephen, ZnO/CdO composite nanorods for photocatalytic degradation of methylene blue under visible light, Mater. Chem. Phys. 125 (2011) 277–280.
[24] P. Wu, T. Komatsu, T. Yashima, IR and MAS NMR studies on the incorporation of aluminum atoms into defect sites of dealuminated mordenites, J. Phys. Chem. 99 (1995) 10923–10931.
[25] M. Burriel, S. Wilkins, J.P. Hill, M.A. Muñoz-Márquez, H.H. Brongersma, J.A. Kilner, M.P. Ryan, S.J. Skinner, Absence of Ni on the outer surface of Sr doped La_2NiO_4 single crystals, Energ. Environ. Sci. 7 (2014) 311–316.
[26] M.S. Park, J.W. Lee, W. Choi, D. Im, S.G. Doo, K.S. Park, On the surface modifications of high-voltage oxide cathodes for lithium-ion batteries: new insight and significant safety improvement, J. Mater. Chem. 20 (2010) 7208–7213.
[27] J. Jun, M. Dhayal, J.H. Shin, Y.H. Han, N. Getoff, Surface chemistry and catalytic activity of Ni/Al_2O_3 irradiated with high-energy electron beam, Appl. Surf. Sci. 254 (2008) 4557–4564.
[28] S.R. Jiang, P.X. Yan, B.X. Feng, X.M. Cai, J. Wang, The response of a NiO_x thin film to a step potential and its electrochromic mechanism, Mater. Chem. Phys. 77 (2003) 384–389.
[29] T. Shishido, T. Tanaka, H. Hattori, State of platinum in zirconium oxide promoted by platinum and sulfate ions, J. Catal. 172 (1997) 24–33.
[30] A. Uheida, M. Iglesias, C. Fontàs, Y. Zhang, M. Muhammed, Adsorption behavior of platinum group metals (Pd, Pt, Rh) on nonylthiourea-coated Fe_3O_4 nanoparticles, Sep. Sci. Technol. 41 (2006) 909–923.
[31] S. Chang, C. Li, K.Y.A. Lin, Comparisons of kinetics, thermodynamics and regeneration of tetramethylammonium hydroxide adsorption in aqueous solution with graphene oxide, zeolite and activated carbon, Appl. Surf. Sci. 326 (2015) 187–194.
[32] V.J. Inglezakis, A.A. Zorpas, Heat of adsorption, adsorption energy and activation energy in adsorption and ion exchange systems, Desalin. Water. Treat. 39 (2012) 149–157.
[33] S. Rengaraj, J.W. Yeon, Y. Kim, Y. Jung, Y.-K. Ha, W.-H. Kim, Adsorption characteristics of Cu(II) onto ion exchange resins 252H and 1500H: kinetics, isotherms and error analysis, J. Hazard. Mater. 143 (2007) 469–477.
[34] V. Gupta, A. Rastogi, Biosorption of hexavalent chromium by raw and acid-treated green alga *Oedogonium hatei* from aqueous solutions, J. Hazard. Mater. 163 (2009) 396–402.
[35] M.E. Argun, S. Dursun, C. Ozdemir, M. Karatas, Heavy metal adsorption by modified oak sawdust: thermodynamics and kinetics, J. Hazard. Mater. 141 (2007) 77–85.
[36] A.A. Jalil, S. Triwahyono, S.H. Adam, N.D. Rahim, M.A.A. Aziz, N.H.H. Hairom, N.A.M. Razali, M.A.Z. Abidin, M.K.A. Mohamadiah, Adsorption of methyl orange from aqueous solution onto calcined Lapindo volcanic mud, J. Hazard. Mater. 181 (2010) 755–762.
[37] K.P. Yadava, B.S. Tyagi, V.N. Singh, Effect of temperature on the removal of lead(II) by adsorption on China clay and wollastonite, J. Chem. Technol. Biotechnol. 51 (1991) 47–60.
[38] N. Unlu, M. Ersoz, Adsorption characteristics of heavy metal ions onto a low cost biopolymeric sorbent from aqueous solutions, J. Hazard. Mater. 136 (2006) 272–280.
[39] R. Celis, M.C. Hermosin, J. Cornejo, Heavy metal adsorption by functionalized clays, Environ. Sci. Technol. 34 (2000) 4593–4599.
[40] F. Ogata, K. Inoue, H. Tominaga, Y. Iwata, A. Ueda, Y. Tanaka, N. Kawasaki, Adsorption of Pt(IV) and Pd(II) from aqueous solution by calcined gibbsite (aluminum hydroxide), e-J. Surf. Sci. Nanotech. 11 (2013) 40–46.
[41] N.N. Nassar, Rapid removal and recovery of Pb(II) from wastewater by magnetic nanoadsorbents, J. Hazard. Mater. 184 (2010) 538–546.
[42] M.M. Benjamin, J.O. Leckie, Multiple-site adsorption of Cd, Cu, Zn, and Pb on amorphous iron oxyhydroxide, J. Colloid Interface Sci. 79 (1981) 209–221.
[43] F. Ogata, N. Kawasaki, Adsorption of Pt(IV) and Pd(II) by calcined dried aluminum hydroxide gel from aqueous solution system, J. Environ. Chem. Eng. 1 (2013) 1013–1019.
[44] A. Uheida, M. Iglesias, C. Fontàs, M. Hidalgo, V. Salvadó, Y. Zhang, M. Muhammed, Sorption of palladium(II), rhodium(III), and platinum(IV) on Fe_3O_4 nanoparticles, J. Colloid Interface Sci. 301 (2006) 402–408.
[45] F. Sabermahani, M. Saeidi, V. Sharifzade, Removal of nickel (II) and palladium (II) from surface waters, Bull. Chem. Soc. Ethiopia 27 (2012) 15–23.
[46] H. Kasaini, M. Goto, S. Furusaki, Selective separation of Pd(II), Rh(III), and Ru(III) ions from a mixed chloride solution using activated carbon pellets, Sep. Sci. Technol. 35 (2000) 1307–1327.
[47] H.W. Ma, X.-p. Liao, X. Liu, B. Shi, Recovery of platinum (IV) and palladium (II) by bayberry tannin immobilized collagen fiber membrane from water solution, J. Membr. Sci. 278 (2006) 373–380.
[48] H. Zheng, D. Zhang, W.Y. Wang, Y.Q. Fan, J. Li, H.P. Han, Highly selective determination of palladium (II) after preconcentration using Pd (II)-imprinted functionalized silica gel sorbent prepared by a surface imprinting technique, Microchim. Acta 157 (2007) 7–11.
[49] Q. Yongchao, H. Yiping, R. Wanlaui, Adsorption behavior of noble metal ions (Au, Ag, Pd) on nanometer-size titanium dioxide with ICP-AES, Anal. Sci. 19 (2003) 1417–1420.
[50] T. Kang, Y. Park, J. Yi, Adsorption behavior of noble metal ions (Au, Ag, Pd) on nanometer-size titanium dioxide with ICP-AES, Anal. Sci. 19 (2003) 1417–1420.